Available online at www.sciencedirect.com

ScienceDirect

Procedia Manufacturing 50 (2020) 401–406

Procedia MANUFACTURING

www.elsevier.com/locate/procedia

18th International Conference Metal Forming 2020

Study of powder densification under hydrostatic loads at high temperatures using finite element method

Borja Elguezabal[a,b,*], Jon Alkorta[a,b], José M. Martínez-Esnaola[a,b], Rafael Soler[c], Estíbaliz Paños[c]

[a]Ceit, Manuel Lardizabal 15, 20018 Donostia / San Sebastián, 20018, Spain
[b]Universidad de Navarra, Tecnun, Manuel Lardizabal 13, 20018 Donostia / San Sebastián, Spain
[c]ITP Aero, Parque Tecnológico nº300, Zamudio, 48170, Spain

* Corresponding author. Tel.: (+34)943212800; fax: (+34)943212800. *E-mail address:* belguezabal@ceit.es

Abstract

Many different constitutive models that describe the behaviour of metal powder during hot isostatic processes are found in literature. A quantitative comparison of these material laws shows a huge discrepancy among the different existing models. This reveals the high sensitivity of the mechanical behaviour of porous materials to the shape, arrangement and distribution of particles and pores.
In order to clarify these discrepancies, the compaction behaviour under high temperature hydrostatic loads for a Nickel-based superalloy has been experimentally characterized. In parallel, three different particle/pore configurations have been analysed at a mesoscopic scale by means of FEM using representative volume elements (RVEs) with periodic boundary conditions. The overall macroscopic response of each RVE has been obtained by a homogenization procedure.
The results confirm the high sensitivity of the overall mechanical response to the microscopic arrangement of pores and particles.

Keywords: Powder compaction; Finite element method; Hydrostatic behaviour; Mesoscopic analysis; Experimental characterization.

1. Introduction

Nowadays, powder metallurgy routes are widely used in the manufacturing of high quality and value components. For example, new alloys developed in the aerospace sector, with higher amounts of strengthening elements, induced the use of powder metallurgy routes due to their extensive segregation and reduction in hot workability [1]. Among the different powder metallurgy processes, Hot Isostatic Pressing (HIP) has been used in industrial applications since the 70s [2]. In this process, the powder is sealed inside a steel container, which is later compacted inside a pressurized vessel of the HIP press, with Argon, which can reach temperatures up to 1500 ºC and pressures up to 200 MPa. During this stage, creep and diffusion ensure that any porosity is eliminated.

In aeronautical applications, the buy-to-fly ratio is commonly used to quantify material efficiency. This parameter is the ratio between the weight of starting raw material and the weight of the final part. Conventional manufacturing routes (casting, forging and machining) have a high buy-to-fly ratio, up to 20:1. With the aim of improving this efficiency Near Net shape processes have been developed. Among these processes, Near Net Shape Hot Isostatic Pressing (NNS-HIP) can achieve high efficiencies with a ratio as low as 1.5:1. This means that every effort to produce a component that is closer to the final configuration will result in a cost reduction – hence the attraction of near-net-shape components [3]

Canister design is an essential task in a near net shape process. The influence of the container geometry and temperature gradients are also relevant to the final deformed shape obtained. These influences have been reported by different authors [4], emphasizing the interest of using accurate numerical models to reduce or eliminate the trial-and-error system in practical cases.

10.1016/j.promfg.2020.08.073

Nomenclature

HIP	Hot Isostatic Pressing
NNS	Near Net Shape
$\boldsymbol{C}_{el}$	Tangent modulus matrix
$\boldsymbol{\sigma}$	Stress tensor
$\mathbf{s}$	Deviatoric stress tensor
$\boldsymbol{\varepsilon}^{e}$	Elastic strain tensor
$\boldsymbol{\varepsilon}^{in}$	Inelastic strain tensor
$\dot{\boldsymbol{\varepsilon}}^{in}$	Inelastic strain rate tensor
I_1	First invariant of stress tensor
J_2	Second invariant of deviatoric stress tensor
σ_y	Yield stress
c	Parameter for deviatoric mechanical behaviour
f	Parameter for hydrostatic mechanical behaviour
ρ_r	Relative density

1.1. Review pressure-dependant material constitutive models

Regarding the modelling of the powder compaction process, historically two different numerical schemes have been employed, which are the Discrete Element Method (DEM) and the Finite Element Method (FEM). In the Discrete Element Method, every powder particle is explicitly considered and its position, velocity and acceleration is numerically computed solving Newton's motion equations. However, it involves a high computational cost, which makes simulating macroscopic systems a difficult task [5-7]. In the Finite Element Method, the powder is modelled as a continuum, the behaviour of which is defined by an adequate material constitutive law.

Plasticity models for porous materials have their origin in the works published by Kuhn and Downey [8] and Green [9]. Several authors have proposed their own yield functions for porous materials, some of them are derived from experimental observations [8, 10, 11, 12] and others from micromechanical considerations [9, 13]. The disadvantages of each model are the lack of general information about the sintering process for the empirical models and the limitation of application to a certain porosity range for the models based on micromechanics. For example, the model proposed by Fleck et al. [13] is suitable only for high porosities, up to the limit of dense random packing of equi-sized spheres. At porosities below about 0.25, the contacts start to interact and the particles become less and less spherical in shape [14].

These models include the dependence upon the hydrostatic pressure and deviatoric stresses (Equation 1). A graphical comparison of these yield surfaces is shown in figure 1, by means of an invariant plane $p-q$, where p and q are calculated as $\sigma_{kk}/3$ and $(3/2 s_{ij}\, s_{ij})^{0.5}$ where $s_{ij} = \sigma_{ij} - 1/3\sigma_{kk}\delta_{ij}$.

$$\phi := AJ_2 + B(I_1)^2 - C(\sigma_y)^2 = 0 \tag{1}$$

where, I_1 and J_2 are the first and second invariant of stress and deviatoric stress tensors respectively and σ_y is the yield stress.

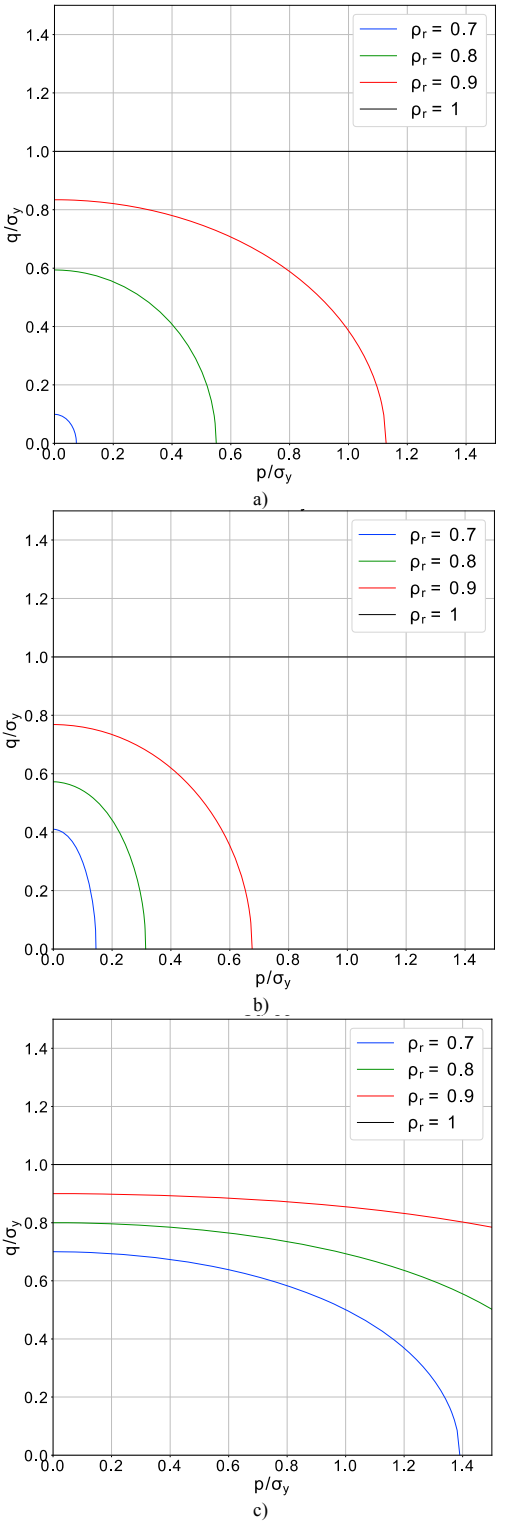

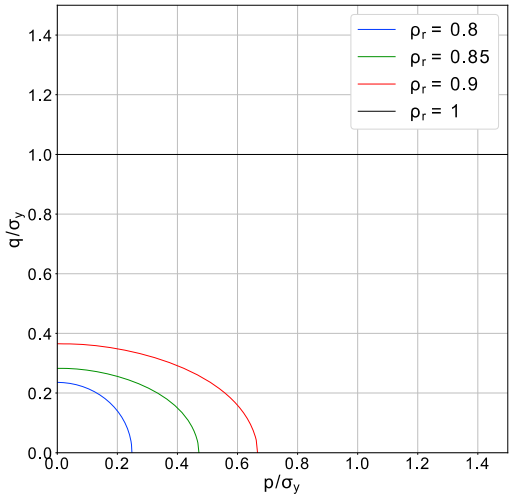

d)

Fig. 1. Yield surfaces of models taken from literature: (a) Doraivelu; (b) Shima & Oyane; (c) Gurson; (d) Abouaf.

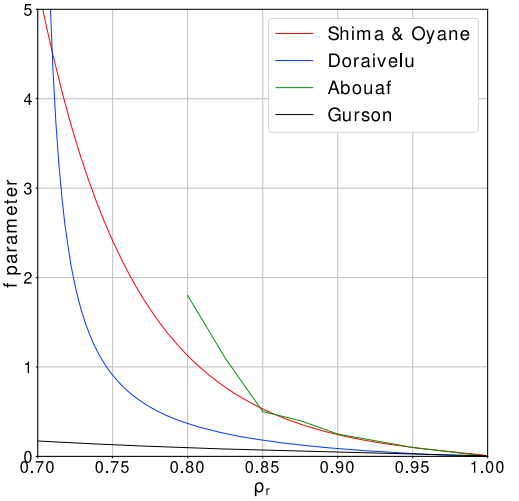

Fig. 2. Comparison of *f* parameter.

Abouaf et al. [2] developed a viscoplastic model to describe the behaviour of the powder during HIP processes. In constitutive models where the deformation is due to plastic or viscoplastic mechanisms, the equivalent stress σ_{eq} is a basic concept, which in this case is defined as follows:

$$\sigma_{eq}^{\ 2} = 3cJ_2 + fI_1^2 \tag{2}$$

where, c and f are material parameters that determine the deviatoric and volumetric behaviour of the powder respectively.

Assuming associativity, a yield surface for Abouaf's viscoplastic model can be derived, which is an ellipse in the invariant plane p-q, as shown in Equation 3.

$$\phi := c\left(\frac{q}{\sigma_y}\right)^2 + 9f\left(\frac{p}{\sigma_y}\right)^2 - 1 = 0 \tag{3}$$

Figure 1 shows that all the yield surfaces present an elliptical or nearly elliptical shape. Therefore, parameter *f* is calculated for the most meaningful cases (see Fig. 2). The huge discrepancy observed between the different existing models reveals the high sensitivity of the mechanical behaviour of porous materials to the shape, arrangement and distribution of particles and pores.

2. Material description

Due to the discrepancies of the different literature constitutive models, the flow behaviour of Astroloy powder is analysed. Astroloy is a Nickel based superalloy, which is usually employed in aeronautical applications. The powder batch has a particle size distribution in the range of 20 to 150 μm.

3. Characterization of parameter *f*

3.1. Experimental set-up and procedure

For the characterization of the *f* parameter, interrupted HIP tests have been carried out in a HIP unit model ASEA QIH-6. In these interrupted HIP tests, the cans are weighted before and after the filling process. In this way, the initial average relative density is calculated. For the powder batch employed, an initial relative density of 0.7 has been measured.

The first step of these interrupted HIP cycles is to heat up the system up to 1000 ºC. This temperature is maintained for 5 minutes to ensure homogenization throughout the solid. Then, hydrostatic pressure is applied at a rate of 2 MPa per minute. Finally, each test is interrupted when the target pressure is reached.

Table 1. Interrupted pressure and temperatures in interrupted HIP cycles.

Target Pressure [MPa]	Temperature [ºC]
10	1000
20	1000
30	1000
35	1000
40	1000
55	1000
70	1000

Specimens of 5 mm in diameter and 10 mm in have been manufactured from partially densified cans. The density of these specimens has been measured by immersion in water, using a scale of high precision.

3.2. Computation of hydrostatic parameter, f, from measured data

For the determination of the f parameter (see Eq. 2), an optimization procedure is implemented consisting of minimizing the error between the numerically and experimentally obtained relative densities. The numerical relative density is computed integrating the temperature-pressure conditions of the interrupted HIP cycle over a single material point for a thermoelastic-viscoplastic law, which is written in Voigt vectorial notation [2]:

$$\boldsymbol{\sigma} = \mathbf{C}_{\mathrm{el}}\left(\boldsymbol{\varepsilon}^{\mathrm{el}} - \frac{1}{3}\ln\left(\frac{\rho_0}{\rho}\right)\mathbf{1}\right)^2 \tag{4}$$

where, $\boldsymbol{C}_{\mathrm{el}}$ is the tangent modulus, $\boldsymbol{\varepsilon}^{\mathrm{e}}$ is the elastic strain vector (assuming small strains), ρ and ρ_0 are the density of dense material at the current temperature, T, and at the initial reference temperature, T_0.

The inelastic strain rate is defined as [2]:

$$\dot{\boldsymbol{\varepsilon}}^{\mathrm{in}} = \mathrm{e}^{\left(A-\frac{QR}{T}\right)}\left[\sinh\left(\alpha\sigma_{\mathrm{eq}}\right)\right]^n\left(\frac{1}{\sigma_{\mathrm{eq}}}\right)\left(\frac{3c}{2}\mathbf{s} + fI_1\mathbf{1}\right) \tag{5}$$

The evolution of the relative density is governed by the material conservation law as follows:

$$\rho_{\mathrm{r}} = \rho_{\mathrm{r0}}\mathrm{e}^{-\mathrm{tr}\left(\boldsymbol{\varepsilon}^{\mathrm{in}}\right)} \tag{6}$$

where ρ_{r0} is the initial relative density of the powder and $\boldsymbol{\varepsilon}^{\mathrm{in}}$ is the inelastic strain vector.

For hydrostatic loads, as in the HIP process, the equation 5 reduces to the following expression:

$$\dot{\boldsymbol{\varepsilon}}^{\mathrm{in}} = \mathrm{e}^{\left(A-\frac{QR}{T}\right)}\sqrt{f}\left[\sinh\left(\alpha p\sqrt{f}\right)\right]^n \tag{7}$$

where p is the applied hydrostatic pressure.

The mentioned constitutive law has been explicitly implemented in a numerical code, with the aim of simulating the HIP cycle, where the material properties and the pressures and temperatures of the cycle are used as input arguments and the relative density of the powder is obtained as output. As it has been mentioned earlier, the material parameters are chosen so as to minimize the error between the numerically and experimentally obtained relative densities. So, the minimization error takes the following form:

$$Error(f) = \sum_i \left(\rho_{\mathrm{r\,num,\,i}} - \rho_{\mathrm{r\,exp,\,i}}\right)^2 \tag{8}$$

As it can be concluded from literature models, the parameter f is a decreasing, smooth and asymptotic function. Because of these properties, the characterized f parameter is fitted to a double potential function.

4. Description of FEM model

Nowadays, the multi-scale approach is well established in the characterization of materials with specific microstructures. The microstructure is usually modelled using a Representative Volume Element (RVE) with periodic boundary conditions (PBCs) so that infinitely large periodic systems can be simulated. Computational homogenization techniques are used to determine the material behaviour on the macroscale [16].

4.1. Geometry

Different geometries have been used to model the powder compaction process at microscopic scale. In the first RVE, a regular and periodic arrangement of equally sized spherical voids is considered. The relative radius of voids determines the overall relative density of the system (Figure 3a). In the second RVE, a regular and periodic arrangement of particles forming a single cubic (SC) structure is considered (see figure 3b). Finally, a Body Center Cubic (BCC) structure has been analysed (Figure 3c).

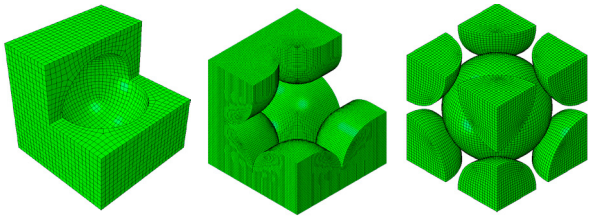

a) b) c)

Fig. 3. (a) Spherical void; (b) SC; (c) BCC.

The analysis of the microscale models has been performed using the commercial finite element package ABAQUS/Standard [17]. A mesh convergence study has been carried out on both models to determine the optimum mesh refinement.

4.2. Material constitutive model

The constitutive model employed is the elastic-viscoplastic model described above. The viscoplastic behaviour has been represented by a creep law of hyperbolic sine type (Equation 5). This model is incorporated among the previously built-in models of ABAQUS.

4.3. Periodic boundary conditions

The boundary conditions of the RVE are generally defined such that the energy equivalence between the two scales, the so called Hill-Mandel condition is preserved [18]. To satisfy this condition the following equation must be fulfilled:

$$\overline{\mathbf{P}} : \dot{\overline{\mathbf{F}}} = \frac{1}{V_0} \int_{V_0} \mathbf{P} : \dot{\mathbf{F}} \mathrm{d}V \tag{9}$$

where $\mathbf{P}$ is the first Piola-Kirchhoff stress tensor, $\mathbf{F}$ is the deformation gradient and V_0 is the volume of the RVE.

Even if several different types of boundary conditions satisfy the Hill-Mandel condition, in this work the periodic displacement and antiperiodic traction boundary conditions are employed.

According to this periodic boundary condition, displacements at the boundaries between two contiguous unit cells must be connected properly to avoid inter-penetration or discontinuities. As a result, a set of linear constraints that relate the relative displacement between nodes located on a pair of opposite surfaces are imposed. In order to impose this relative displacement in the finite element model, three reference nodes (also known as dummy nodes) are included in the model.

4.4. Contact properties

During the compaction process, the particles come into contact. During contact at high temperature, diffusion phenomena leads to the formation of necks and the particles are welded to each other. Therefore, the FE model considers no slip between particles in contact. In addition, in the normal direction, penetration is prevented by a hard type contact.

4.5. Homogenization

A homogenization procedure has been applied to obtain the macroscopic stress and strain tensors. In this homogenization procedure, which is based on the work of Loidolt [19], the macroscopic stress tensor is computed from the forces taken from the reference nodes and the current cross-sectional areas.

$$\boldsymbol{\sigma} = \begin{bmatrix} \frac{F_{xx}}{A_x} & \frac{F_{xy}}{A_x} & \frac{F_{xz}}{A_x} \\ \frac{F_{yx}}{A_y} & \frac{F_{yy}}{A_y} & \frac{F_{yz}}{A_y} \\ \frac{F_{zx}}{A_z} & \frac{F_{zy}}{A_z} & \frac{F_{zz}}{A_z} \end{bmatrix} \tag{10}$$

where F_{ij} represent the force in the node i in the direction j, and A_k is the plane with normal direction k.

Regarding the macroscopic strain tensor, due to the large strains developed in the powder compaction, the finite strain Green-Lagrange tensor is used. Finally, the relative density is computed directly from its definition, as the ratio of the amount of volume that is material to the total volume of the RVE cube.

4.6. Simulation strategy for estimation of flow parameters

For the estimation of f, a purely hydrostatic stress state has been imposed on the mesoscopic model. For this purpose, the same magnitude of displacement has been imposed on each reference node in the direction normal to the pair of surfaces to which they are related. From the homogenization procedure, σ-$\sigma - \dot{\varepsilon}^{\mathrm{in}} - \rho_r$ data points are computed. Introducing these points in Abouaf's model particularized for the hydrostatic case, an equation is obtained (Equation 7), where the only unknown is the value of f, which has been solved numerically. This procedure is repeated every desired relative density value.

5. Results and discussion

The experimentally obtained results have been compared with models from bibliography. In Figure 4, the experimental results are compared with Abouaf [2], Gurson [15] and Doraivelu [11] models. As shown in the figure, the experimental results are in an intermediate position between Abouaf and Gurson models.

As can be seen in Figure 4, as far as mesoscopic models are concerned, the spherical pore model does not correctly represent the behaviour of the powder in a hydrostatic stress state. This should not be surprising since spherical pores are not expected during powder compaction processes. The results are in good agreement with Gurson's model (that is based on a spherical void configuration) and confirm the high stability of spherical pores, which offer a high resistance to be deformed volumetrically. For this reason, the values of parameter f obtained for this model are lower than those obtained experimentally.

With regard to both configurations of the spherical particles, it is observed that the results obtained are quite similar to the experimental ones, especially at high relative densities. The difference in f at low densities may be due to the fact that, with this model, no relocation of the powder particles in the initial stages of the compaction process is considered.

A comparison of the results obtained from the mesoscopic models against the values extracted from literature models has been done. As can be concluded from Figure 4, the mesoscopic

spherical pore model and Gurson's model show almost identical behavior under hydrostatic stress. This is due to the fact that Gurson extracted his constitutive law from the analytical approach of a pore of elliptical shape in a continuous medium [15]. It should also be noted the similarity between the results obtained in the BCC configuration and the model postulated by Doraivelu.

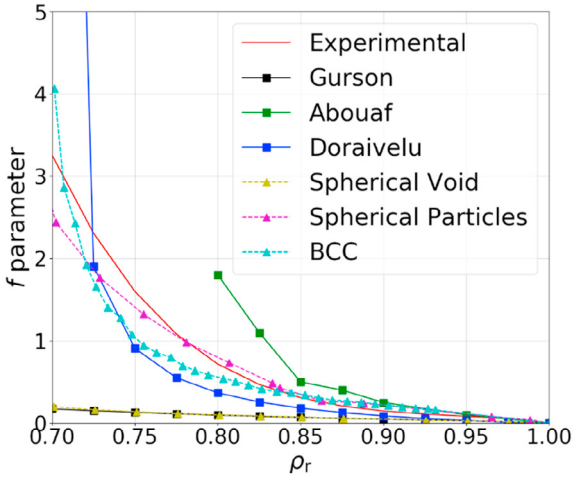

Fig. 4. Comparison of mesoscopic results and constitutive models from literature.

6. Conclusion and outlook

Nowadays there are several constitutive laws to model the behaviour of metallurgical powders during their compaction. However, there are great differences among their behavioural predictions. The results obtained in this work together with the literature models reviewed indicate that the response of porous materials to external stresses is very sensitive to the shape and arrangement of pores. This work shows that spherical pores (concave pore surfaces) are very stable under external hydrostatic stresses that lead to low values of *f*. On the other hand, the voids left by spherical particles (convex in shape) are less stable, more prone to densification (higher values of *f*). The experimental results of partially densified samples manufactured by means of interrupted HIP tests confirm the lower stability of the latter configuration.

Finally, a mesoscopic analysis has been performed using FEM models. In these models, three completely different configurations have been used to model the representative volume element. Of the geometries investigated, the geometries using spherical powder particles arrangements are the ones that best fits the experiment mesurements. However, little discrepancies are recorded at low relative densities. These discrepancies are attributed to the fact that the phenomenon of rearrangement of particles in the early stages of the compaction process is not included in the mesoscopic models.

Acknowledgements

The project leading to this application has received funding from the Clean Sky 2 Joint Undertaking under the European Union's Horizon 2020 research and innovation programme (Call Reference N°: JTI-CS2-2017-CfP07-ENG-03-22) under grant agreement No [821044]

References

[1] Furren D, Noel J. Evaluation of P/M U720 for gas turbine engine disk application, TMS; 1996. p. 705-711.
[2] Abouaf M, Chenot JL, Raisson G, Bauduin P. Finite element simulation of hot isostatic pressing of metal powders. Int J Numer Meth Engi 1988;25:191-212.
[3] Dutta B, Froes FH. Titanium powder metallurgy. In Qian M, Froes FH, editors. Amsterdam: Elsevier; 2015. p. 447-468.
[4] Abouaf M, Chenot JL, Raisson G, Bauduin P. Prediction of the deformation during the production of near net shape superalloy parts by hot isostatic pressing. 2nd International Conference on Isostatic Pressing, Stratford-on-Avon; 1982. p. 21-23.
[5] Redanz P, Fleck N. The compaction of a random distribution of metal cylinders by the discrete element method. Acta Mater 2001; 49:4325-35.
[6] Persson AS, Frenning G. An experimental evaluation of discrete element simulations of confined powder compression using an extended truncated-sphere model. Powder Technol 2015;284:257-64.
[7] He Y, Wang Z, Evans TJ, Yu AB, Yang RY. DEM study of the mechanical strength of iron ore compacts. Int J Mineral Process 2015;142;73-81.
[8] Kuhn HA, Downey CL. Deformation characteristics and plasticity theory of sintered powder materials. Int J Powder Metall 1971;7:15.
[9] Green RJ. A plasticity theory for porous solids. Int J Mech Sci 1972;14:215-24.
[10] Shima S, Oyane M. Plasticity theory for porous metals. Int J Mech Sci 1976;18:285-91.
[11] Doraivelu S, Gegel H, Gunasekera J. A new yield function for compressible P\M materials. International Journal of Mechanical Sciences 1984; 26: 9-10.
[12] Corapcioglu MY, Uz T. Constitutive equations for plastic deformation of porous materials. Powder Technol 1978;21:269-274.
[13] Fleck NA, Kuhn LT, McMeeking RM. Yielding of metal powder bonded by isolated contacts. Journal of the Mechanics and Physics of Solids 1992; 40:1139-1162.
[14] Redanz P. Numerical modelling of the powder compaction of a cup. European J Mech - A/Solids 1999;8:399-413.
[15] Gurson AL, Continuum Theory of Ductile Rupture by Void Nucleation and Growth: Part I- Yield criteria and Flow Rules for Porous Ductile Media. J Eng Mater Tech 1977;99:2-15.
[16] Garoz D, Gilabert FA, Sevenois RDB, Spronk SWF, Van Paepegem W. Consistent application of periodic boundary conditions in implicit and explicit finite element simulations of damage in composites. Composites Part B 2019; 168: 254-266.
[17] Dassault Systèmes. ABAQUS Documentation. Providence, RI, USA.
[18] Hill R. Elastic properties of reinforced solids: some theoretical principles. J Mech Phys Solids 1963;11:357-72.
[19] Loidolt P, Ulz MH, Khinast J. Modeling yield properties of compacted powder using a multi-particle finite element model with cohesive contacts. Powder Technol 2018;336:426-40.